Physicochem. Probl. Miner. Process., 61(4), 2025, 205443

http://www.journalssystem.com/ppmp

Physicochemical Problems of Mineral Processing

ISSN 1643-1049

Separation mechanism and kinematic characteristics of particles on screen panel with different vibration modes

Tao Wu [1,2], Sanpeng Gong [1,3], Guofeng Zhao [1,3], Ningning Xu [1,3], Bowei Liu [1], Fuqiang Zhang[1]

[1] School of Mechanical and Power Engineering, Henan Polytechnic University, Jiaozuo 454003, China

[2] Zeptool Co., Ltd., Tongling 244000, China

[3] Henan Province Engineering Technology Research Center for Coal Mine Mechanical Equipment Jiaozuo 454003, China

Corresponding author: 18813089516@163.com (Sanpeng Gong)

Abstract: Vibrating screens are critical equipment for achieving effective mineral classification and clean, efficient utilization. The motion characteristics of particles on screen panels under different vibration modes significantly influence their screening efficiency and processing capacity. However, there is limited research on the separation mechanism and kinematic characteristics of particle systems on screen panels. In this study, explicit dynamics particle generation technology was employed to establish a kinematic simulation model of the screen panel and particle system using the finite element method (FEM) and discrete element method (DEM). The separation mechanism of particle systems on screens with different vibration modes was described from a macroscopic physical perspective. The dynamic characteristics of particles in various size fractions on the screen were analyzed, and the influence law of mineral particle mass on the kinematic characteristics of screening equipment was explored. The research results indicate that during the screening process, particles achieve the separation of materials with different particle sizes on the screen through percolation and convection mechanisms. The vibrating flip-flow screen (VFFS) can achieve particle separation more rapidly than traditional vibrating screens. Moreover, when the mass of mineral particles on the screen panel increases, the activity of particles on the VFFS panel is most significantly affected. The time required for fine particles on the screen panel with different vibration modes to completely pass through the screen increases linearly with the increasing mass.

Keywords: separation mechanism, kinematic characteristics, screen panel, vibration modes, FEM-DEM coupling

1. Introduction

As a vital component of the world's energy resources, coal plays a significant role. Screening serves as a key foundational process for the efficient processing and clean utilization of coal resources (Yu et al., 2023; Zi et al., 2025). The effectiveness of coal screening is highly dependent on the vibration mode of the screen panel. Aiming at the problem of agglomeration and caking of wet and fine particles on the screen panel in traditional screening, the common approach is to increase the vibration intensity of the screen panel (Duan et al., 2021; Moraes et al., 2022). By doing so, the cohesive forces between the aggregated fine particles can be broken, achieving the effect of separating the agglomerates. However, an overly high vibration intensity will impose a burden on the structural strength of the screening equipment, making it prone to damage. There-fore, theoretically analyzing the separation patterns of the granular material and exploring its kinematic characteristics to reveal the mechanism of mineral screening has drawn considerable attention from numerous scholars (Kopacz et al., 2017; Gong et al., 2020; Li et al., 2021; Wang et al., 2022).

Researchers have focused on investigating particle separation behavior and mechanisms by leveraging mineral properties and vibration parameters. Vorster W analyzed the upward movement of

DOI: 10.37190/ppmp/205443

coarse particles in vibrating sand through combined experimental and practical approaches, reducing the randomness of fine particle separation by amplifying harmonic oscillations (Vorster et al., 2002). Liao utilized the phenomenon where fine particles fill voids created by rising coarse particles to elaborate on the relationship between particle size and percolation mechanism (Liao, 2016). Zhao investigated the cohesive forces and separation behavior of particles under vertical vibration modes, explaining the influence of cohesion on separation patterns (Zhao et al., 2019). Amir M analyzed the effects of vibration amplitude on particle mixing and separation, finding results that were qualitatively consistent with previous experimental and numerical studies (Amir et al., 2019). However, these mechanistic studies mainly focus on physical phenomena of particle systems and have not yet explored the dynamic characteristics of particle-system coupling with screen panels.

As the effect of the material group on the screen panel cannot be ignored, relevant scholars have employed the discrete element method to study the dynamic characteristics of the coupling system between particles and the screen panel. Dong et al. simulated the motion characteristics of particles on a multi-layer banana screen based on the discrete element method and analyzed the influence rules of the screen hole shape and system parameters on the screening efficiency (Dong et al., 2017). Davoodi et al. (2019a; 2019b) used the discrete element method to analyze the influence characteristics of screen plates made of different materials on the material screening process and explored the influence rules of factors such as material fluidity and screen hole shape on the screening performance. Aghlmandi et al. (2018) carried out numerical simulations on industrial vibrating screens, analyzed the influence rules of system parameters on the screening efficiency of particles with different shapes, and verified the rationality of the simulations through screening experiments. It can be seen that the discrete element method can effectively simulate the kinematic characteristics of particles during the screening process on a rigid screen panel. However, Conventional DEM has deficiencies in coupling with structural mechanics as it fails to accurately describe energy dissipation and transfer between the flexible structure and particles. Thus, it is difficult to use it to analyze the dynamic characteristics of the coupled system of the flexible VFFS panel and the material group.

Researchers such as Wu et al. (2019) and Zhang et al. (2019) conducted approximate flexibility treatment on VFFS panels based on catenary theory, and carried out co-simulations of the two-way coupling characteristics between granular materials and VFFS panels using EDEM and RecurDyn software. They analyzed the influence rules of eccentric mass, screen inclination angle, and feed particle size composition on screening efficiency, productivity, and particle movement velocity (Wu et al., 2019; Zhang et al., 2019). Due to certain errors in approximating the motion of elastic screen panels, Chen et al. combined the advantages of FEM and DEM to propose a FEM-DEM coupled simulation method capable of describing the dynamic characteristics of VFFS under heavy loads. This method was used to investigate the motion trajectory of single particles on VFFS and the influence characteristics of screen acceleration on particle motion and screen penetration (Chen et al., 2021). Although various studies have been conducted on particle stratification and motion characteristics of vibrating screens, there is a lack of comprehensive analysis that clarifies the separation mechanisms and motion characteristics of particle groups on screens with different vibration modes, as well as the integrated analysis of motion laws caused by different vibration modes.

In response to the deficiencies in the aforementioned research, this paper constructs a simulation model of the dynamic characteristics of the coupling system between the screen panel and the material group under different vibration modes based on the FEM-DEM coupling method. It comparatively analyzes the macroscopic physical phenomena of the spatial motion of particles on the screen panel under different vibration modes, and explores the dynamic characteristics of particles on the screen under the influence of different vibration modes from a microscopic perspective. The energy changes in the screening system are used to explain the influence of the screen panel motion mode on the particle activity, and the changes in the motion laws of the particle group on the screen caused by the increase in the unit processing mass of the screen panel are investigated. The study reveals that different vibration modes of the screen panel significantly influence the size separation and kinematic characteristics of particles on the screen panel, thereby providing a theoretical basis for selecting appropriate screening modes and structures according to the characteristics of different materials to be screened, thereby achieving the optimal screening performance.

2. Coupled simulation model of particles and screen panel with different vibration modes

2.1. The joint simulation principle of FEM-DEM

By integrating the advantages of the FEM and DEM, this approach can effectively simulate interparticle contact motions and interactions between particles and screen panels (Jiang et al., 2017a; 2017b). While simulating screen panel movements under different vibration modes, it achieves bidirectional coupling data transmission between particles and the screen. The joint simulation analysis principle of the two methods is illustrated in Fig. 1.

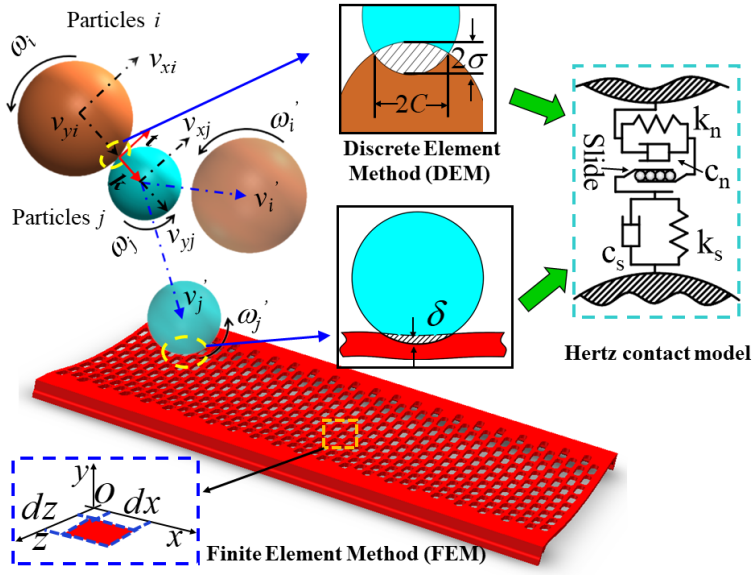

Fig. 1. Principle of FEM-DEM joint simulation

The FEM-DEM coupling approach centers on Hertz contact theory, using the screen panel micro-element as the fundamental research unit. The relationships among displacement, stress, and strain can be expressed by Eq. 1 (Zheng et al., 2017):

$$\begin{Bmatrix}\varepsilon_x\\ \varepsilon_y\\ \varepsilon_z\\ \gamma_{xy}\\ \gamma_{yz}\\ \gamma_{zx}\end{Bmatrix}=\begin{bmatrix}\partial/\partial x & 0 & 0\\ 0 & \partial/\partial y & 0\\ 0 & 0 & \partial/\partial z\\ \partial/\partial y & \partial/\partial x & 0\\ 0 & \partial/\partial z & \partial/\partial y\\ \partial/\partial z & 0 & \partial/\partial x\end{bmatrix}\begin{Bmatrix}u\\ v\\ w\end{Bmatrix}=\begin{bmatrix}\frac{1}{E_x} & \frac{-\mu_{yx}}{E_y} & \frac{-\mu_{zx}}{E_z} & 0 & 0 & 0\\ \frac{-\mu_{xy}}{E_x} & \frac{1}{E_y} & \frac{-\mu_{zy}}{E_z} & 0 & 0 & 0\\ \frac{-\mu_{xz}}{E_x} & \frac{-\mu_{yz}}{E_y} & \frac{1}{E_z} & 0 & 0 & 0\\ 0 & 0 & 0 & \frac{1}{G_{xy}} & 0 & 0\\ 0 & 0 & 0 & 0 & \frac{1}{G_{yz}} & 0\\ 0 & 0 & 0 & 0 & 0 & \frac{1}{G_{zx}}\end{bmatrix}\begin{Bmatrix}\sigma_x\\ \sigma_y\\ \sigma_z\\ \tau_{xy}\\ \tau_{yz}\\ \tau_{zx}\end{Bmatrix} \quad (1)$$

where ε_x, ε_y, ε_z, γ_{xy}, γ_{yz}, and γ_{zx} stand for normal strain and shear components in x, y, and z directions, respectively (P_a). σ_x, σ_y, σ_z, τ_{xy}, τ_{yz}, and τ_{zx} represent normal stress and shear stress components in the x, y, and z directions, respectively (P_a). u, v, and w are the displacements in the x, y, and z directions, respectively (mm). E_x, E_y, and E_z stand for the elasticity moduli for length, width, and thickness (Pa). Equations $G_{xy} = \sqrt{E_x E_y}/2(1+\sqrt{\mu_{xy}\mu_{yx}})$ and the Poisson's ratio (μ_{xy}, μ_{yz}, μ_{zx}) are used to compute the screen plate's shear modulus, denoted as G_{xy}, G_{yz}, and G_{zx}.

When the screen panel is loaded with granular material, to investigate dynamic parameters such as displacement and velocity between particles under working conditions, considering the gravitational and collision forces acting on the particles during motion, the motion equations between particles can be derived based on Newton's second law (Jafari et al., 2016):

$$\begin{cases} m_i \dfrac{d^2 \boldsymbol{S}_i}{dt^2} = \sum_j^{n_i} (\boldsymbol{F}_{cn,ij} + \boldsymbol{F}_{ct,ij}) + \boldsymbol{F}_{g,i} \\ I_i \dfrac{d\boldsymbol{\alpha}_i}{dt} = \sum_j^{n_i} (\boldsymbol{T}_{ij}^{n} + \boldsymbol{T}_{ij}^{s}) \end{cases} \tag{2}$$

Here m_i is the mass of particle I (kg). $\boldsymbol{S_i}$ represent its displacement deformation (mm). $\boldsymbol{F}_{cn,ij}$ and $\boldsymbol{F}_{ct,ij}$ stand for the normal and tangential collision forces of particle i and j, respectively (N). $\boldsymbol{F}_{g,i}$ is the gravitational force of particle i (N). I_i represent its moment of inertia (mm⁴). $\boldsymbol{\alpha}_i$ stands for its rotation angle (°), $\boldsymbol{T}_{ij}{}^{n}$ and $\boldsymbol{T}_{ij}{}^{s}$ stands for the normal and tangential moments of particle i and j collision, respectively (N·mm), and n_i is the total number of particles in contact with particle i.

Considering the complexity of particle group collisions, it is assumed that only two-body collisions exist in the particle system. The Hertz-Mindlin contact model is adopted, and the contact force between particles is described by a spring-damper model in the normal direction and a spring-damper-slider model in the tangential direction.

$$\begin{cases} \boldsymbol{F}_{cn,ij} = -c_n \boldsymbol{v}_{n,ij} - k_n \delta \\ \boldsymbol{F}_{ct,ij} = -c_t \boldsymbol{v}_{t,ij} - k_t C \end{cases} \tag{3}$$

where c and k stand for the material's damping coefficient and stiffness (N/mm), respectively. δ and C are the normal and tangential displacement deformation of the collision between particles (mm). $\boldsymbol{v}_{ij}$ represents the relative velocity between the particles (mm/s).

Using the soft-sphere model with a certain penetration amount at the contact panel, as shown in Fig. 1, the influence of tangential forces between the two colliding particles on normal motion is negligible and can be reasonably omitted. Thus, the relationship between contact force variation and relative velocity under maximum overlap can be derived from Hertz contact theory (Hertz, 1882):

$$F_n = \frac{4}{3}\left[\frac{15(m_i + m_j) E^{*\frac{2}{3}} \sqrt{R}^{\frac{2}{3}} \boldsymbol{v}_{ij}{}^2}{16 m_i m_j}\right]^{\frac{3}{5}} \tag{4}$$

where $E^* = 1/\left[\left(\frac{1-\mu_i{}^2}{E_i}\right) + \left(\frac{1-\mu_i{}^2}{E_j}\right)\right]$ and $R = r_i r_j/(r_i + r_j)$ with E_i, μ_i, r_i, and E_j, μ_j, r_j being the elastic modulus, Poisson's ratio, and radius between various particles, respectively. Therefore, the inelastic collision time of two particles can be obtained using the theory of elasticity (Alobaid et al., 2014):

$$t_c = 1.47\left[\frac{15 m_i m_j}{16(m_i + m_j) E^* \sqrt{R}}\right]^{\frac{5}{2}} \frac{1}{|\boldsymbol{v}_{ij}|^{\frac{1}{5}}} \left(1 + \frac{1}{e^{\frac{1}{5}}}\right) \tag{4}$$

Here, e is the elastic recovery coefficient.

The relative velocity of the two particles after collision can be expressed as $\boldsymbol{v}_{ij}{}' = -e\boldsymbol{v}_{ij}$, and the tangential velocity component before and after the collision is identical in size and direction, the impulse before and after particle collision can be obtained written as:

$$-m_i(\boldsymbol{v}_i' - \boldsymbol{v}_i) = m_j(\boldsymbol{v}_j' - \boldsymbol{v}_j) = \boldsymbol{J} \tag{6}$$

where $\boldsymbol{J}$ is the impulse of the collision particle (N/s). $\boldsymbol{v'}$ is the particle's velocity after collision (mm/s).

Eq. 7 can then be used to determine the particles' post-collision velocity:

$$\begin{cases} v_i' = v_i - \dfrac{(1+e) m_j}{(m_j + m_i)} (\mathbf{k} \cdot v_{ij}) \mathbf{k} \\ v_j' = v_j + \dfrac{(1+e) m_i}{(m_j + m_i)} (\mathbf{k} \cdot v_{ij}) \mathbf{k} \end{cases} \tag{7}$$

where **k** represents the particle's relative velocity's normal unit vector.

According to the law of conservation of energy, the energy dissipation during the collision can be obtained by the difference in total kinetic energy of the two-particle system before and after the collision:

$$\Delta E = \frac{1}{2} \frac{m_i m_j}{m_i + m_j} \left(1 - e^2\right) |\boldsymbol{v}_{ij}|^2 \tag{8}$$

To better describe the contact between particles and the screen panel, the screen is modeled as a particle with an infinite radius. According to the inter-particle collision theory, substituting into Eq. 3

yields the collision force between the screen and particles:

$$\lim_{r_i\to\infty}F_n=\lim_{r_i\to\infty}\frac{4}{3}\left[\frac{15(m_1+m_j)E^{*\frac{2}{3}}\sqrt{\frac{r_ir_j}{r_i+r_j}}^{\frac{2}{3}}\boldsymbol{v}_{ij}^{\ 2}}{16m_1m_j}\right]^{\frac{3}{5}}=\frac{4}{3}\left[\frac{15(m_1+m_j)E^{*\frac{2}{3}}\sqrt{r_j}^{\frac{2}{3}}\boldsymbol{v}_{ij}^{\ 2}}{16m_1m_j}\right]^{\frac{3}{5}} \tag{9}$$

where m_1 is the mass of the screen panel. Also, Eq. 10 can be used to express the length of time that particles and the screen panel are in contact:

$$\lim_{r_i\to\infty}t_c=1.47\left[\frac{15m_im_j}{16(m_i+m_j)E^*\sqrt{r_j}}\right]^{\frac{5}{2}}\frac{1}{|\boldsymbol{v}_{ij}|^{\frac{1}{5}}}\left(1+\frac{1}{e^{\frac{1}{5}}}\right) \tag{10}$$

The collision mechanism between the screen panel and the particles has a theoretical foundation according to the mathematical model mentioned above.

2.2. Establishment of the simulation model

Based on the above contact models between particles and between particles and the screen panel, the screen panel motion modes of three types of screening equipment, namely VFFS, circular vibrating screens (CVS), and linear vibrating screens (LVS), were selected as the research objects. Simulations were conducted using ABAQUS finite element software to construct a single screen plate for describing the motion behavior of particle groups on each screen panel. The parameters of the simulation model are listed in Table 1.

To ensure data accuracy, the screen panels are uniformly made of polyurethane material. In constructing the simulation model, the material properties of the VFFS panel are described using the Mooney-Rivlin model, with two parameters in the model strain energy density function being C_{01}=0.7 MPa and C_{10}=2.8 MPa. The CVS and LVS panels undergo global rigidification treatment. Harmonic displacement load excitation is applied to the screen panels based on the motion patterns of different screening equipment, described by the equation $f(x)$=Asin(ωt). The loads applied to the screen panel of the VFFS are located at both ends of the screen panel, facing each other in a straight line and pointing towards the center of the screen panel. The linear screen load is positioned at the bottom of the screen panel, directed vertically upward. The CVS uses combined synchronous normal and tangential loads to achieve circular trajectory motion.

Table 1. Physical parameters of the simulation model

Physical Parameters	Value
Size of screen panel/mm	300×328 ×4
Amplitude A/mm	6
Angular frequency ω/ rad·s^{-1}	75.36
Material density of screen panel/kg·mm^{-3}	1.35×10^{-6}

Table 2. Physical property parameters of selected minerals

Particle properties	Numerical value
Density / kg·mm^{-3}	1.43×10^{-6}
E/Mpa	1200
μ	0.25
e	0.35

To conserve computational resources, hexahedral elements are employed for screen panel meshing, simulating the kinematic characteristics of screens with different vibration modes under no-load conditions. Particle generation technology in explicit dynamics analysis is utilized to generate particles above the screen panel through coding, enabling FEM-DEM coupling. The friction coefficients between mineral particles, between particles and the screen panel, and between particles and baffles are 0.45, 0.48, and 0.63, respectively. The particle numbers are 5000 per square meter, and the radii of the particles

are 3 mm, 6.5 mm, and 12.5 mm, with their proportions being 40%, 30%, and 30%, respectively. Mineral properties are listed in Table 2. The technical flow is shown in Fig. 2, with a total simulation duration of 10.5 s.

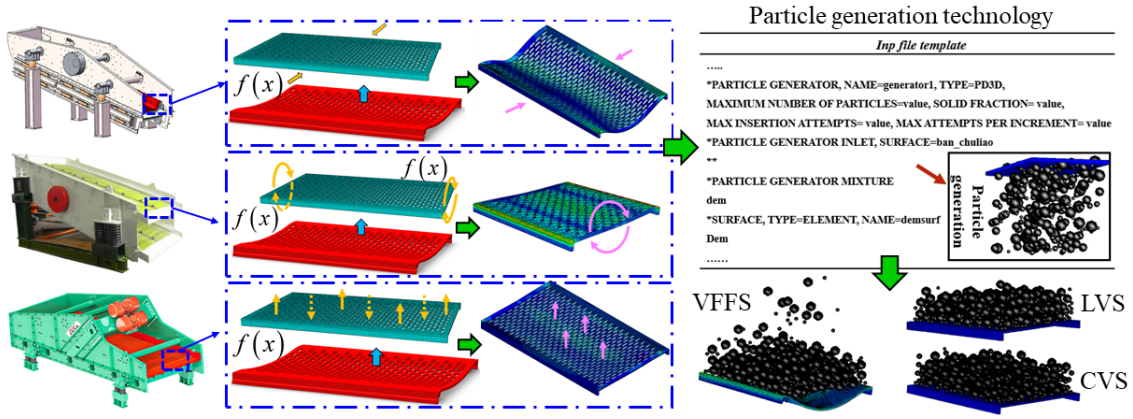

Fig. 2. Simulation process of linkage between screen panel and particle population under various vibration modes

3. Simulation analysis and results discussion

3.1. Separation of particle populations

The particle volume packing fraction (D_v) is introduced to visually describe the spatio-temporal distribution of particles on the screen panel $D_v=V_q/V_s$, where V_q is the total particle volume and V_s is the spatial volume occupied by the particle distribution. Through calculation, the static D_v of mineral particles with the same volume on each screen is 39.4%. When the time reaches 2 sec, the particles on the screens with different vibration modes tend to move steadily. The curves of D_v varying with time are obtained, as shown in Fig. 3.

During motion, the D_v is significantly reduced. The D_v curves of CVS and LVS exhibit similar fluctuation ranges, distributed within the interval of 15%-20%. However, a sudden change occurs at 7 s, which is attributed to the momentary suspension of individual fine particles and can be considered negligible. The D_v of VFFS ranges from 2% to 4%.

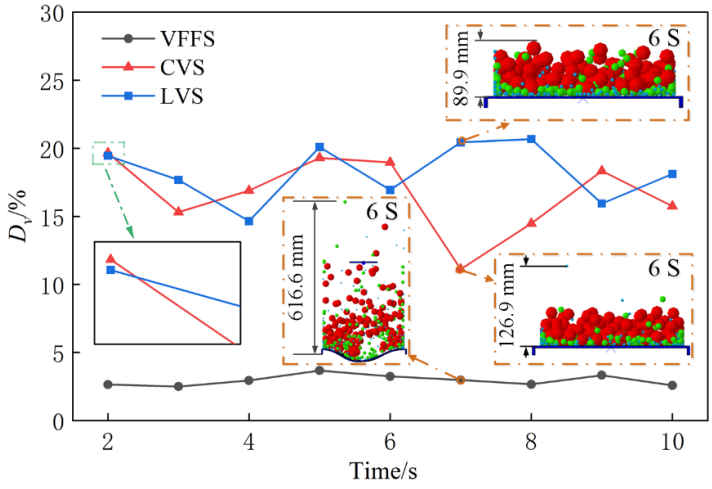

Fig. 3. The volume packing fraction of particles on the screen panel under different vibration modes

The results indicate that when the screen panel undergoes forced vibration, it promotes the rupture of contact force chains among accumulated particles, leading to spatial volume expansion of particles on the screen and a reduction in D_v. Significant disparities in D_v exist under different vibration modes: VFFS exhibit smaller D_v values with larger interparticle gaps, which facilitate the passage of other particle size fractions through these gaps to reach the bottom and make contact with the screen panel.

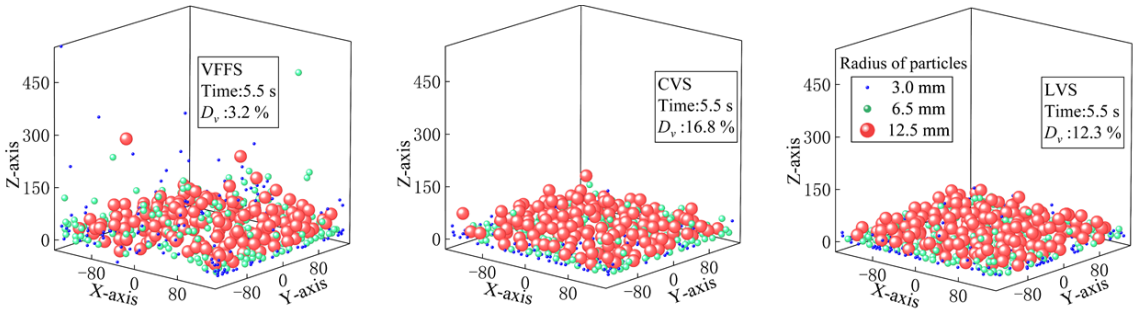

Fig. 4. The instant motion of particles on the screen panel in various vibration modes

The spatial states of particles on the screen panel under different vibration modes are shown in Fig. 4. Significant differences in particle distribution are observed across varying D_v values: particles on VFFS exhibit high mobility, with medium-to-fine size fractions randomly distributed in the screen space, while CVS and LVS feature small inter-particle gaps, where fine particles percolate to the bottom, forming a segregation phenomenon.

This indicates that VFFS promotes active particle motion with large spacing, facilitating fine particle penetration through gaps to contact the screen panel. This increases contact frequency between sub-mesh particles and the screen, enhancing effective screening probability. Additionally, large particle spacing reduces collision probability during motion, minimizing energy loss. Although CVS and LVS achieve distinct particle segregation, their lower particle mobility and small spacing increase kinetic energy dissipation and hinder fine particle penetration. Consequently, VFFS contacts more particles of diverse sizes than the other two screen types within the same timeframe, resulting in relatively higher screening efficiency.

The penetration movement of fine particles through the gaps to the bottom of the screen panel explains the movement phenomenon of particles on the VFFS. However, this penetration movement fails to clarify the phenomenon that for CVS and LVS, although the inter-particle spacing on the screen is small and some fine particles cannot pass through the gaps, a full separation of particles of various size fractions is still achieved. To further explore the principle of particle separation on the screen, by utilizing the changes in the displacement vectors of particle movement on the screen, schematic diagrams of particle movement were drawn for the top-view of the screen and the cross-sections at 20 mm, 150 mm, and 280 mm along the length direction under different vibration modes in a stable state, as shown in Fig. 5.

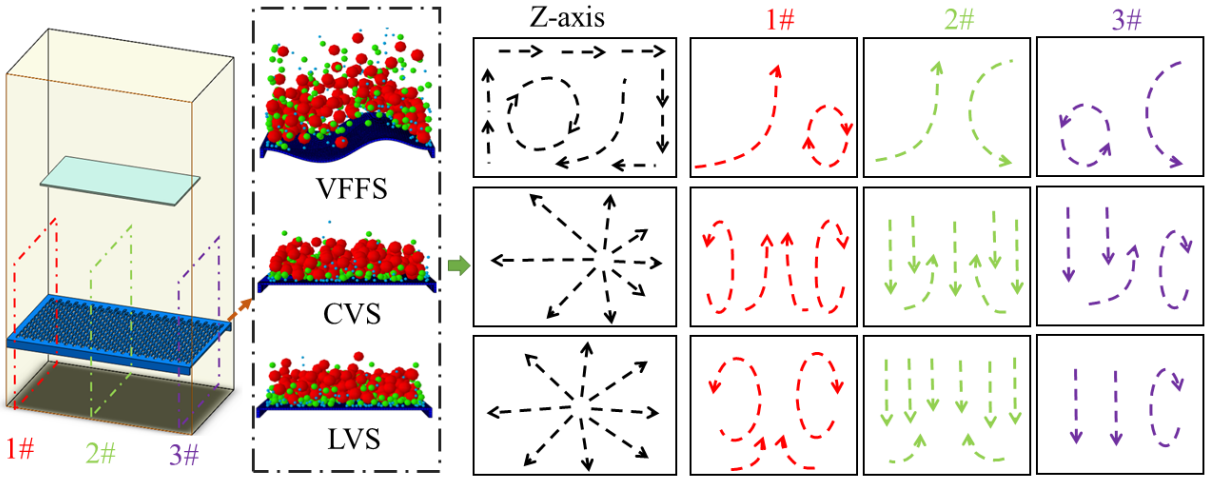

Fig. 5. Diagrammatic representation of particle motion in various vibration modes. Z-axis is the top view. 1# is where the profile is located at 20 mm along the screen panel's length direction. 2# is where the profile is located at 150 mm along the screen panel's length direction. 3# is where the profile is located at 280 mm along the screen panel's length direction

As shown in Fig. 5, particles on the three types of screen panels with different vibration modes all move upward at the center of the screen panel and downward near the screen edges. On the upper panel of the particle layer, particles move from the central protrusion of the container towards the screen edges. The VFFS forms local small-scale convection at the edges and is susceptible to impact from ascending particle flows, while CVS and LVS develop convection loops on their front and rear sides. The results indicate that due to its material properties and large deflection deformation, the VFFS transmits substantial energy to particles, leading to high particle velocities and chaotic motion. This chaotic motion disrupts inter-particle convection, making it difficult for particles of the same size fraction to agglomerate through convective movement. In contrast, the relatively lower energy transfer in CVS and LVS promotes the evolution of material particles towards ordered and organized global convection, resulting in the separation of particles of the same size. This indirectly reflects that CVS and LVS are more conducive to regular particle motion on the screen panel.

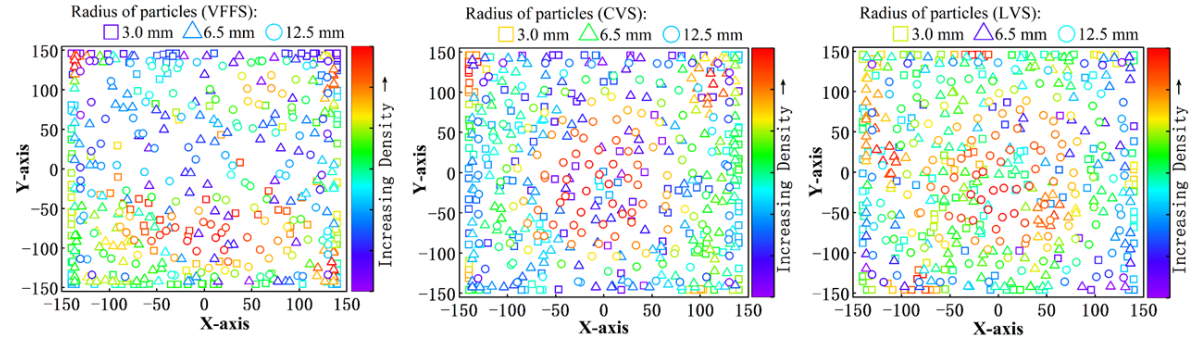

(a) The screen's particle population's motion state at 3.0 seconds with various vibration patterns

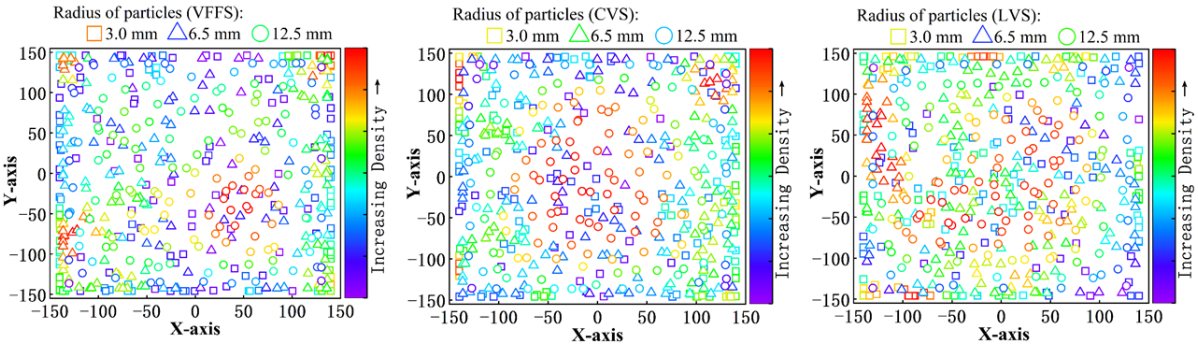

(b) The screen's particle population's motion state at 3.083 seconds with various vibration patterns

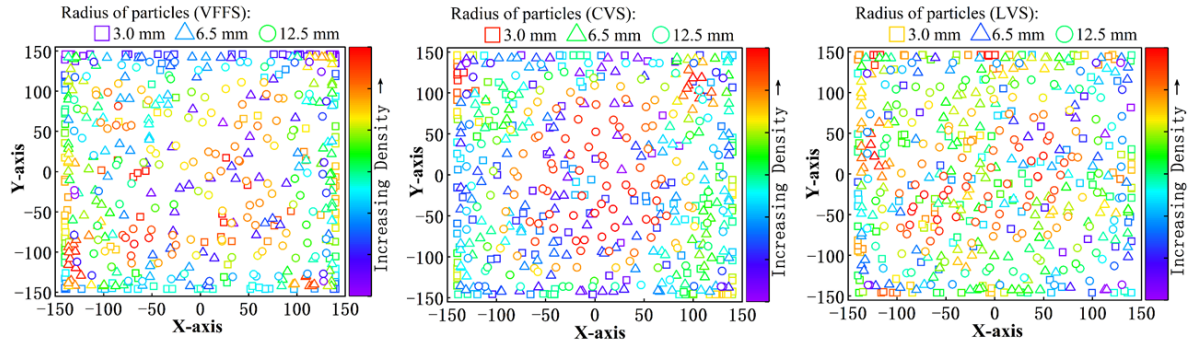

Fig. 6. Particle population scattering density distribution for various vibration modes: (c) The screen's particle population's motion state at 3.15 seconds with various vibration patterns

To investigate the influence of the convection mechanism of particle groups on their separation characteristics, particle analysis was conducted over three screen motion cycles, and scatter density distribution maps of particles on the screen were created, as shown in Fig. 6.

As indicated by Fig. 6, within different cycles of the VFFS particle system, substantial changes in particle density distribution occur with complex motion migration. At the local scale, particles of the

same size fraction exhibit minor agglomeration behavior over short time intervals. For CVS and LVS, large particles are concentrated in broader regions, with small particles on circular screens forming aggregates in narrow edge areas, while small particle density distributions on linear screens are relatively uniform.

Studies on particle segregation characteristics over different vibrating screens reveal that particle motion on VFFS is complex and variable, with particle migration primarily occurring through inter-particle gap penetration. For CVS and LVS, large particles move to the upper layer of the screen frame space through convection, restricted by particle radius and unable to move towards the screen bottom along the convection loop, thus forming separation of same-sized particles. The distinct screen motion patterns significantly affect the distribution of particles within the same size fraction.

3.2. Kinematic characteristics of particles

The above studies provided a macroscopic description of the physical phenomena of particle system motion on screens with different vibration modes. To gain a deeper understanding from a microscopic perspective, it is essential to analyze the dynamic characteristics of particles on screens under different vibration modes by delving into their motion behaviors. Time-displacement curves of particles of various size fractions on different vibrating screens were plotted (Fig. 7) by extracting displacement time data of particles at steady state, averaging the results for particles of the same size fraction, and graphing the motion trajectories.

As can be seen from Fig. 7, the fluctuation range of the particle system on the VFFS panel is 26.85 mm, 91.02 mm, and the displacement curves of particles of various size fractions intersect and overlap with each other in the time domain. For the CVS and LVS, the displacement range of large particles on the screen is 25.14 mm, 35.87 mm, which does not overlap with the ranges of particles of other size fractions. In Fig. 7b, when comparing the curves of fine particles on the screen under different vibration modes, the fluctuation of the average displacement of fine particles on the VFFS is much higher than that on CVS and LVS. Although CVS and LVS have different motion modes, the displacement curves of their fine particles are similar, and the average displacement is adjacent to the fluctuation range of the screen panel.

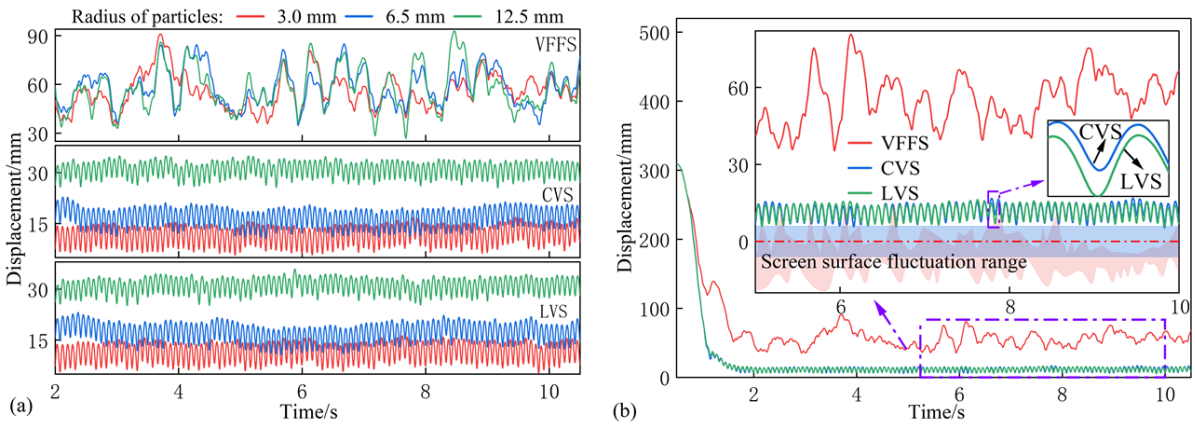

Fig. 7. Particle populations' kinematic characteristics when subjected to various vibration modes: (a) Particle kinematic graphs for various particle sizes (b) Kinematic trajectory of a 3 mm radius particle

The results indicate that the large deflection deformation of the screen panel causes particles of various sizes on the VFFS to distribute over a wider interval. The probability of newly fed particles and moving particles downward at the feed end penetrating the over-screen particle bed to contact the screen surface is higher than that in CVS and LVS. Moreover, in the early stage, particles of all size fractions exhibit more contact behavior with the screen panel within a shorter time, which is conducive to fine particle passage through the screen. However, once the particle motion stabilizes and size separation occurs on CVS and LVS, this advantage diminishes. Since size separation requires a certain time, CVS and LVS necessitate a lower flow velocity of the particle population to achieve complete screening.

3.3. Analysis of the energy of particle collisions

During the movement of particles in the space above the screen, energy is transferred between particles and between particles and the screen surface. To explore the differences in the movement of particles on the screen caused by the different energy transfer between the screen surfaces with different vibration modes and particles, on the premise of ensuring accuracy, the assumption of binary collisions between particles mentioned above is adopted. Thus, the relative velocity between particles remains constant. By substituting the parameters of the mineral particles in Table 2 into Eqs. 4 and 8 in Section 2, the relationships between the particle radius, collision force, and energy loss are plotted, as shown in Figs. 8 and 9.

As shown in Figs. 8, 9, the collision force between two particles is positively correlated with particle radius: larger particle size fractions generate greater collision forces and correspondingly higher energy losses. For cases with a large size difference, both collision force and energy loss are smaller. Combining with Eq. 6, it can be derived that the velocity difference of small particles before and after collision is higher than that of large particles. The higher post-collision velocities of small particles partially explain the particle size separation phenomenon observed on the screen panel.

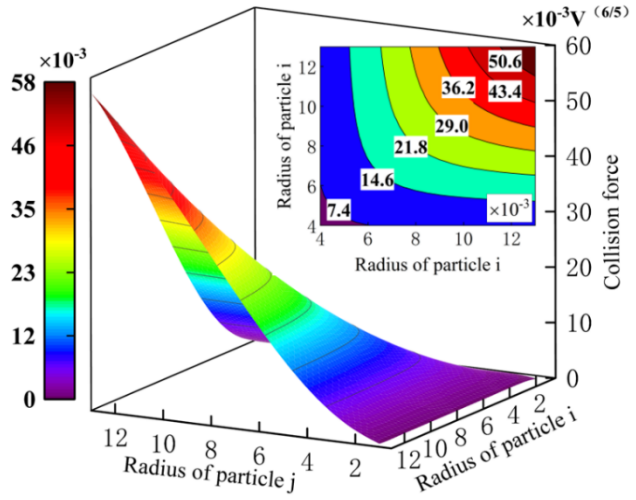

Fig. 8. Variations in particle radius and collision force

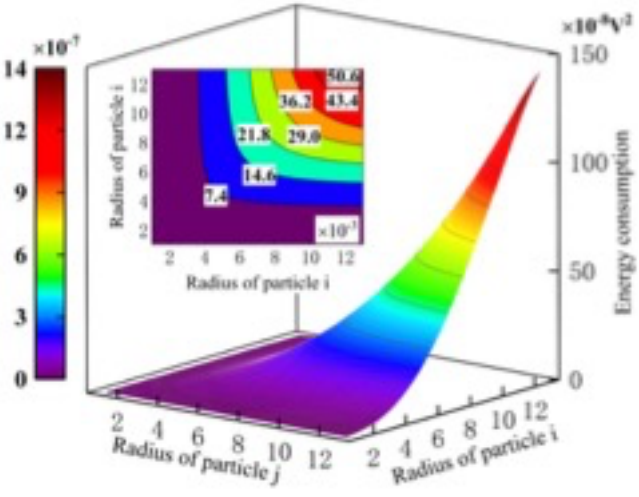

Fig. 9. Variation in energy loss and particle radius

The vibration intensity Γ ($\Gamma = 4\pi^2 f^2/g$), where f is vibration frequency, L is amplitude, and g is gravitational acceleration) is introduced as a critical indicator influencing energy transfer between the screen panel and particles. Through numerical calculations of screen motion, the Γ value for the VFFS under no-load conditions is 30.7 g, while CVS and LVS exhibit Γ values of 3.29 g. The larger Γ of the

VFFS results in greater collision forces and energy consumption during particle contact. Using numerical simulation data, system kinetic energy curves under different vibration modes are plotted, as shown in Fig. 10.

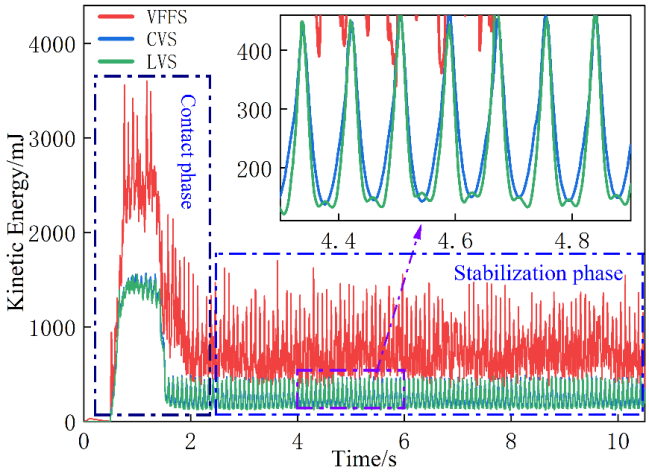

Fig. 10. Kinetic energy curve of screen panel under various vibration modes

In Fig. 10, during the contact phase, all kinetic energy curves first increase and then decrease. When particles contact the screen panel, collision-generated energy causes the curves to rise. The system kinetic energy curve reaches its peak when the number of particles in contact with the screen is constant. As particle input continues, energy dissipation increases, leading to a downward trend in the kinetic energy curve. After the particle input stops at the feeding end, the system curve gradually stabilizes.

During the steady-state phase, CVS and LVS exhibit similar kinetic energy curve variations, with their fluctuation ranges accounting for 25.68%-28.34% of the VFFS's kinetic energy. Moreover, the upper limit of the kinetic energy variation range for CVS and LVS only reaches the lower limit of the VFFS's range. This indicates that the VFFS motion transfers significantly more energy to the particle system, resulting in screen-particle relative velocities much higher than those of CVS and LVS. Consequently, particle displacements on the VFFS are distributed over a broader spatial range.

3.4. Effect of change in particle population mass on the kinematic characteristics of screening systems

Based on the contact phase in the kinetic energy variation curves, when the mass on the screen increases, the kinetic energy curve fluctuates significantly. To clarify the influence of different screen material masses on the kinematic characteristics of screening, comparative experiments were designed for screens with different vibration modes under three groups of processing masses: 23.94 kg·m^{-2}, 47.87 kg·m^{-2}, and 71.81 kg·m^{-2}.

When the screen processing capacity increases equivalently, the static D_v of the particle system increases by 9.2% and 16.7%, respectively. Small particles partially fill the gaps between large particles, promoting an upward trend in static D_v, as shown in Fig. 11b. When screens with different processing capacities are subjected to forced vibration, their D_v variation curves are presented in Fig. 11a.

As shown in Fig. 11a, the D_v curve of the VFFS exhibits the most significant variation, with an increase in amplitude of 63%-87%. The D_v changes on CVS and LVS are similar, showing an increase range of 14%-45%.

This indicates that as the screen processing capacity increases, the dynamic D_v of particles under working conditions approaches the static value. When the dynamic D_v equals the static value, the screen processing capacity reaches its theoretical limit. Based on the D_v mapped mobility, variations in mass have the most significant impact on material mobility on the VFFS. Moreover, the influence of screen material mass on particle system mobility under different vibration modes follows a logarithmic trend: as mass increases, the reduction in mobility becomes smaller.

Based on the minimum potential energy principle, when the entire system tends towards equilibrium, fine particles on the screen move to the lowest point to make contact with the screen panel.

For different processing capacities, displacement time curves depicting the motion characteristics of particles on screens under different vibration modes are plotted, as shown in Fig. 12.

In Figs. 12(a) and (c), for the VFFS, displacement curves of particles in different size fractions separate as the processing mass increases, and this separation becomes more pronounced with higher mass. For the CVS, the displacement range of large particles on the screen expands from 36.7 mm, 42.34 mm to 39.3 mm, 44.53 mm over time, while displacement ranges of other size fractions shift downward, and the time required for the displacement curves to reach steady state increases. LVS exhibits the same pattern of variation.

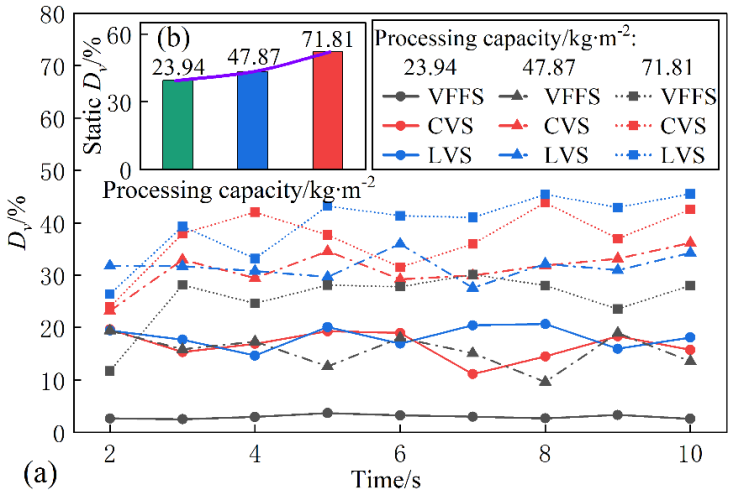

Fig. 11. Variation of D_v with different vibration modes and processing capacity on the screen panel: (a) Columnar trend chart of the static D_v of particles under different processing capacities of the screen panel (b) The variation curves of particle D_v under different vibration modes

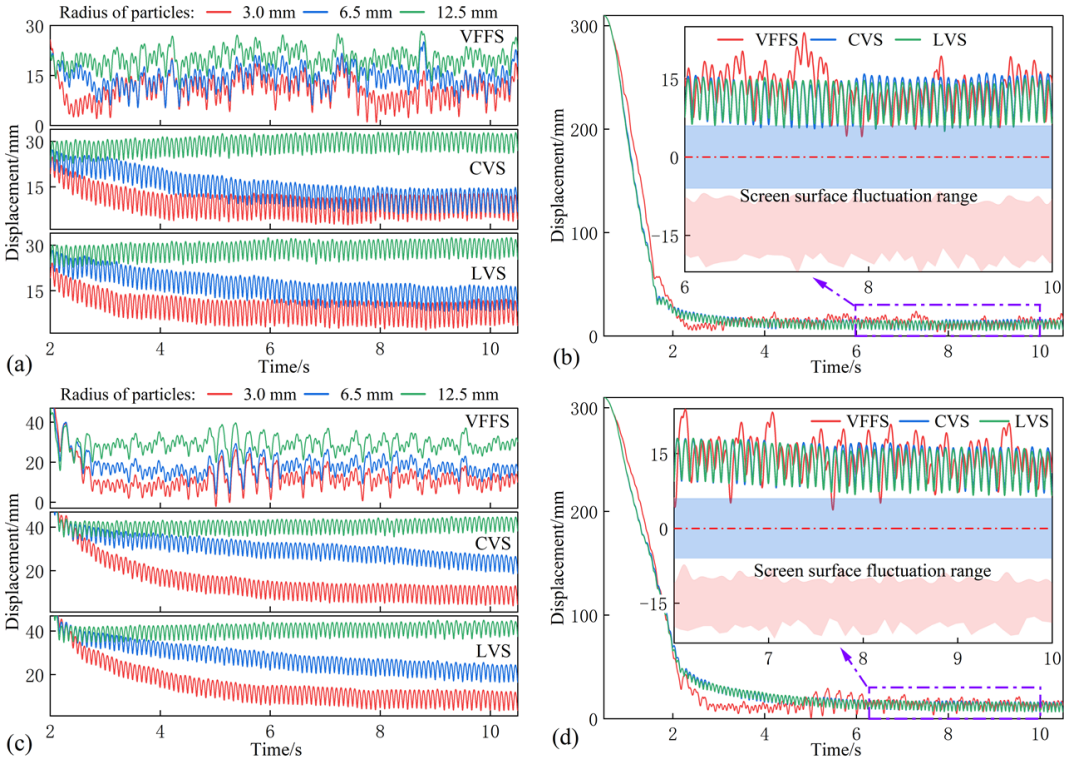

Fig. 12. Particle populations' kinematic characteristics on screens with various vibration modes as the mass varies: (a) The unit particle population on the screen panel has a mass of 47.87 kg·m^{-2} (c) The unit particle population on the screen panel has a mass of 71.81 kg·m^{-2}. The motion characteristics of 3 mm-sized particles in various particle population masses are shown in (b) and (d)

Figs. 12(b), (d), and Fig. 9(b) show the displacement changes of fine particles on each screen under different processing masses. The time corresponding to the stabilization of the displacement curves of fine particles under different vibration modes was recorded. The relationship between the time required for fine particles on the screen to reach a steady-state motion and different processing loads was fitted by the least-squares method, as shown in Table 3. The results indicate that there is a linear relationship between the increase in the processing mass on the screen and the time for fine particles to reach a steady state. CVS and LVS exhibit longer stabilization times for fine particles on the screen, resulting in fewer contacts between fine particles and the screen panel during the unsteady period compared to VFFS. However, when the processing mass on VFFS increases, the screen deformation amplitude L decreases by over 55%, leading to a reduction in Γ and corresponding decreases in particle mobility on the screen. Additionally, excessive loading causes VFFS to remain in a tensile state for extended periods, reducing its service life compared to linear and CVS.

Table 3. The length of time needed for small particles to stabilize in various vibration modes

Mass of particles on the screen per unit area	VFFS/s	LVS/s	CVS/s
23.94 kg·m^{-2}	1.61	2.0	1.73
47.87 kg·m^{-2}	2.42	3.4	4.07
71.81 kg·m^{-2}	3.43	5.92	6.08
Fitted slope	0.91	1.96	2.18

Time-domain displacement data of particle systems on screens under different vibration modes were analyzed, and Fourier transforms were applied to the data to obtain amplitude curves in the frequency domain. The frequency spectrogram is presented in Fig. 13.

The amplitude variations corresponding to different screen vibration modes exhibit significant differences in frequency. For CVS and LVS, the frequency corresponding to the maximum particle amplitude coincides with the screen fundamental frequency. Within the same screen motion mode, as the particle size fraction increases, the corresponding primary amplitude decreases. VFFS demonstrates lower particle amplitudes at the screen fundamental frequency position, with complex frequency compositions. As screen processing mass increases, vibration amplitudes of particles in various size fractions change significantly, and the particle amplitude corresponding to the screen fundamental frequency increases.

This indicates that external harmonic excitation provides primary energy for particle motion on CVS and LVS. During the motion of VFFS, large deflection deformation occurs, resulting in different energy transfer at various contact positions with particles. This leads to complex amplitude compositions of particle frequencies distributed over a broader real number domain, increasing the probability of resonance due to overlapping with the natural frequencies of other particles on the screen and thus enhancing material fluidity. For a processing mass of 71.81 kg·m^{-2}, the frequency spectrogram of 6.5 mm particles on CVS and LVS exhibits significant amplitudes in the low-frequency region, which can be explained by the unsteady displacement curves of 6.5 mm particles on both vibrating screens shown in Fig. 12c.

As indicated by the above analysis, with increasing processing mass on each screen, the steady-state phase on the screen exhibits a phenomenon where large particles occupy the upper layer while fine particles settle in the lower layer. Changes in volume packing fraction indicate small inter-particle gaps, and particles of various size fractions display similar periodic motion patterns on screens with different vibration modes.

To deeply investigate the motion of particle systems on screens with different vibration modes as a function of processing mass variation, corresponding two-dimensional phase space trajectory plots and Poincaré section diagrams were generated based on time displacement curves of particle systems under varying processing capacities for different vibration modes, as shown in Fig. 14.

The results indicate that the phase trajectory curves of particle systems on CVS and LVS asymptotically stabilize into closed curves. As screen processing capacity increases, trajectories evolve from multiplication loops to convergent limit cycles. However, during the large deflection deformation of VFFS in contact with particles, complex energy exchange from collisions disrupts this asymptotic

stability. When the screen material mass increases, particle mobility decreases, causing the particle system to stabilize again.

Using stroboscopic sampling with the external excitation frequency as the sampling period, Poincaré scatter plots are distributed across the two-dimensional plane. Poincaré section diagrams reveal that particles on CVS and LVS exhibit distinct quasi-periodic motion, with this approximation strengthening as screen mass increases. In contrast, Poincaré scatter plots of VFFS particles disperse across the plane,

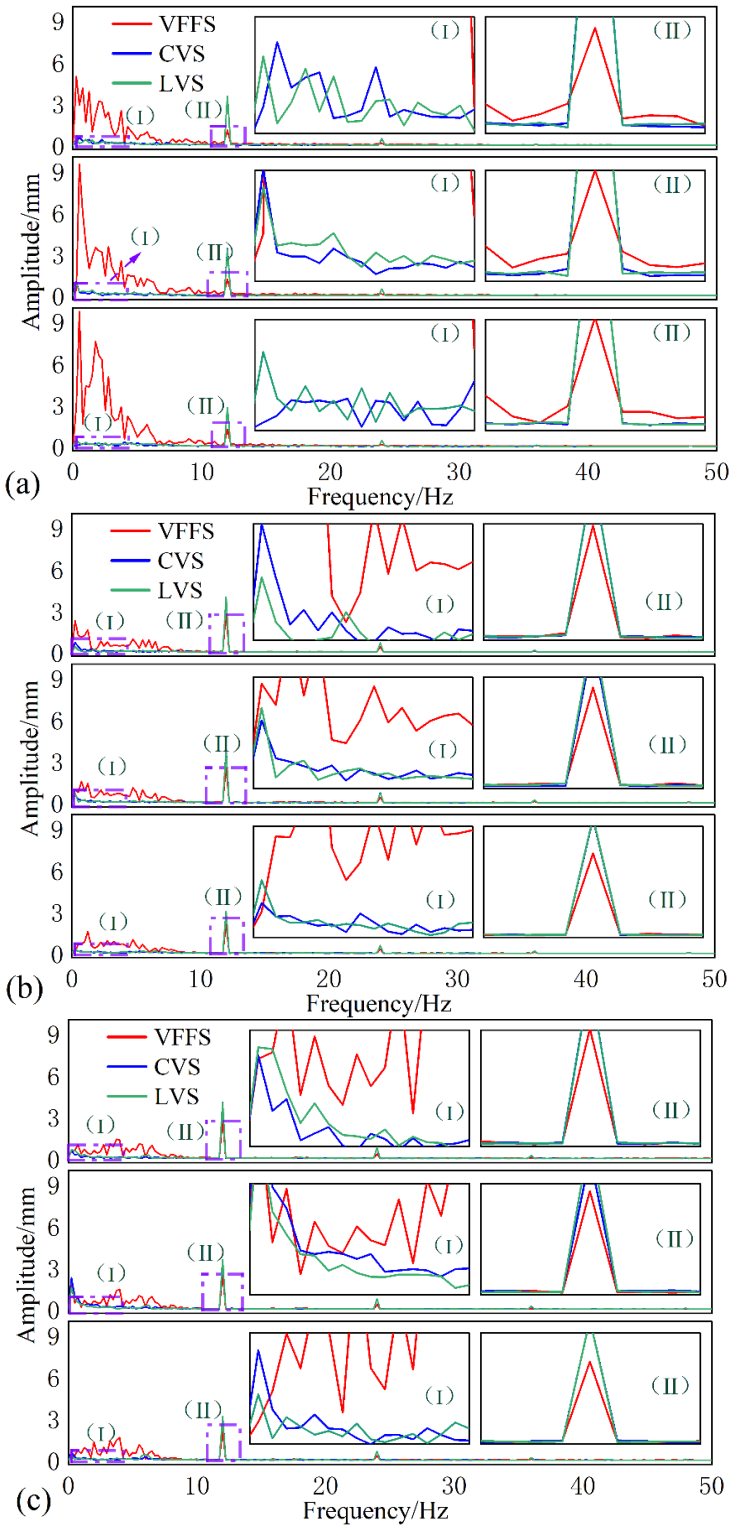

Fig. 13. The motion spectrum map of particles for each size particle for various vibration modes under various particle population mass differences: (a), (b), and (c) stand for 23.94 kg·m^{-2}, 47.87 kg·m^{-2}, and 71.81 kg·m^{-2}, respectively, the mass of the particle population per unit area on the screen

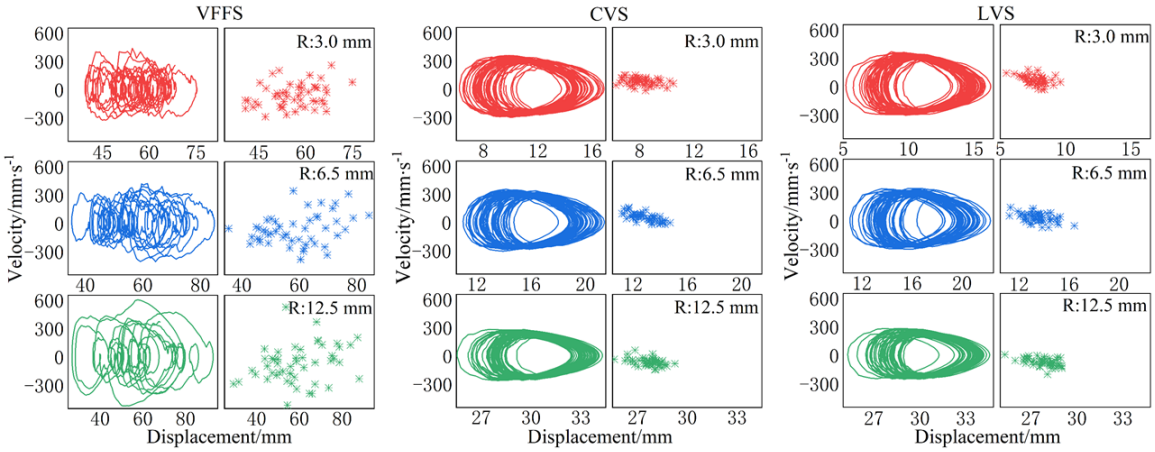

(a) The unit particle population on the screen panel has a mass of 23.94 kg·m-2

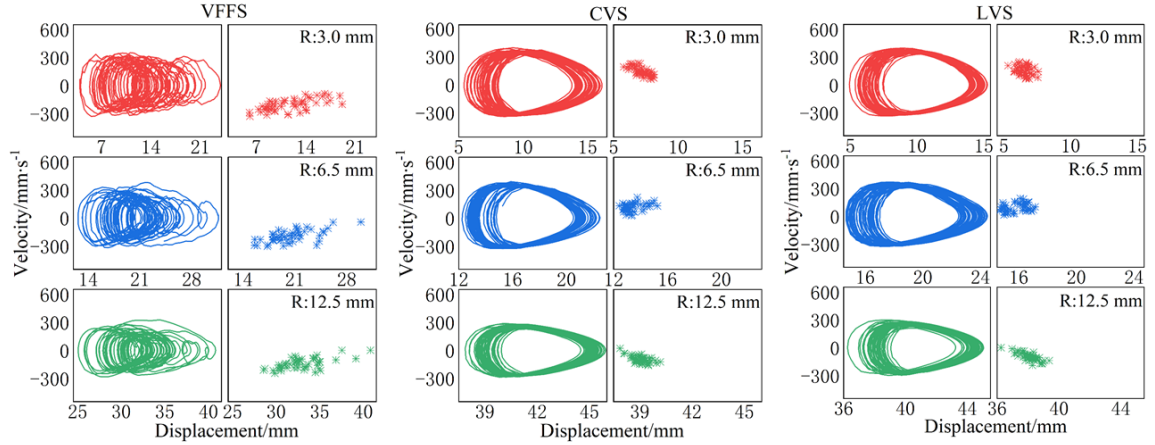

(b) The unit particle population on the screen panel has a mass of 47.87 kg·m-2

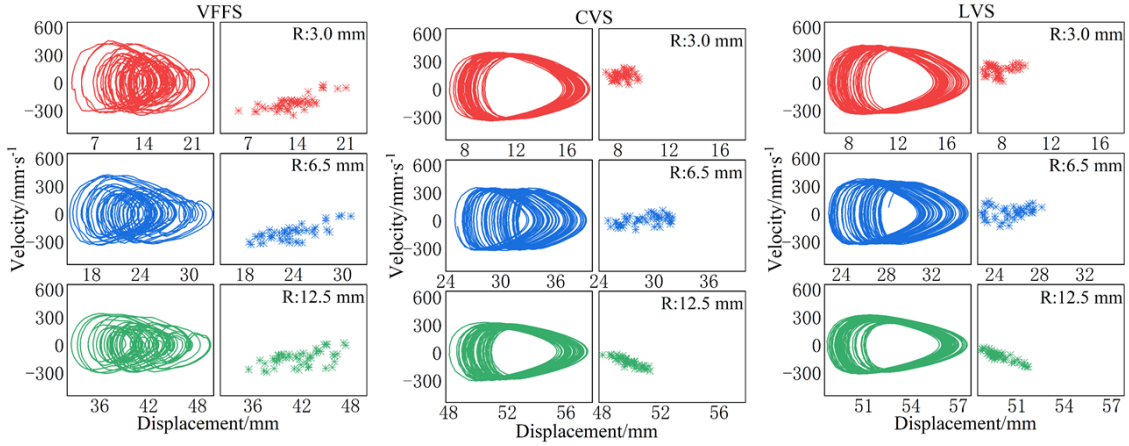

Fig. 14. Poincaré cross section and kinematic phase diagram for particle population mass difference: (c) The unit particle population on the screen panel has a mass of 71.81 kg·m-2

transitioning from period-doubling bifurcation to chaotic motion. The entire particle system exhibits sensitive dependence on initial conditions. When screen processing capacity increases, the Poincaré plots show a transition from chaotic to quasi-periodic motion, causing VFFS particles to lose high mobility and form accumulations on the screen panel.

Therefore, different vibration modes of the screen panel have significant impacts on particle size separation and motion characteristics on the screen. Consequently, vibration modes should be rationally selected based on the characteristics of the material to be screened and the structural requirements of the screening equipment to achieve optimal screening performance.

4. Conclusions

Based on collision and Hertzian theories, inter-particle contacts and motion patterns were investigated. Additionally, the evolutionary mechanisms of particle segregation on the screen panel were investigated from two dimensions: physical phenomena and dynamic analysis, revealing the influence of the processing capacity of minerals on the screening performance. The main conclusions can be summarized as follows:

Mineral particles achieve size separation on screens with different vibration modes through percolation and convection. The screen panel of the VFFS transfers greater energy via particle collisions, resulting in a higher relative velocity. Within a shorter timeframe, the VFFS screen panel contacts more fine particles than LVS and CVS. In contrast, full contact between fine particles and the screen panel on CVS and LVS requires a lower particle flow velocity on the screen panel.

The relationship among the particle radius, the collision force, and the energy loss is intuitively expressed through formulas, illustrating that the difference in particle size grades is positively correlated with the velocity difference before and after particle collisions. As the mass of the particle population on the screen increases, particle mobility decreases, prolonging the time required for fine particles to fully contact the screen bottom, which exhibits a linear relationship. The time sequence for fine particles to fully contact the screen under different vibration modes is: CVS > LVS > VFFS. An increase in screen processing mass causes the amplitude attenuation of the VFFS screen panel to exceed 55%, having the most significant impact.

The amplitudes of particle motion on CVS and LVS derive from external harmonic excitation and remain relatively stable. The large deflection deformation of VFFS panels provides significant motion amplitudes to particles but is highly influenced by the screen processing mass. As processing mass increases, the particle system on VFFS transitions from non-periodic to quasi-periodic motion, prone to forming accumulations.

The research achievement can not only enrich the theory of mineral screening, but also provide a theoretical basis for the selection of the required screening equipment for different minerals. Moreover, it offers a theoretical foundation for the optimization of the comprehensive performance of screening equipment.

Acknowledgments

The research is financially supported by the National Natural Science Foundation of China (52204267), the Key Scientific and Technological Project of Henan Province (252102221006, 242102220007, 252102221005), and the Discipline Innovation and Intelligence Introduction Program of Higher Education Institutions (25A460013).

References

AGHLMANDI HARZANAGH, A., ORHAN, E.C., ERGUN, S.L., 2018. *Discrete element modelling of vibrating screens*. Minerals Engineering 121, 107–121.

ALOBAID, F., BARAKI, N., EPPLE, B., 2014. *Investigation into improving the efficiency and accuracy of CFD/DEM simulations*. Particuology, 16, 41–53.

CHEN, B., YU, C., GONG, S., WANG, X., 2021. *Dynamic characteristics of LIWELL flip-flow screen panel and particle movement*. Chemical Engineering Science, 245, 116853.

DAVOODI, ALI, ASBJÖRNSSON, G., HULTHÉN, E., EVERTSSON, M., 2019a. *Application of the discrete element method to study the effects of stream characteristics on screening performance*. Minerals, 9, 788.

DAVOODI, A., BENGTSSON, M., HULTHÉN, E., EVERTSSON, C.M., 2019b. *Effects of screen decks' aperture shapes and materials on screening efficiency*. Minerals Engineering 139, 105699.

DONG, K., ESFANDIARY, A.H., YU, A.B., 2017. *Discrete particle simulation of particle flow and separation on a vibrating screen: Effect of aperture shape*. Powder Technology, 314, 195–202.

DUAN, C., YUAN, J., PAN, M., HUANG, T., JIANG, H., ZHAO, Y., QIAO, J., WANG, W., YU, S., LU, J., 2021. *Variable elliptical vibrating screen: Particles kinematics and industrial application*. International Journal of Mining Science and Technology, 31, 1013–1022.

GONG, S., OBERST, S., WANG, X., 2020. *An experimentally validated rubber shear spring model for vibrating flip-flow*

screens. Mechanical Systems and Signal Processing, 139, 106619.

JAFARI, A., SALJOOGHI NEZHAD, V., 2016. *Employing DEM to study the impact of different parameters on the screening efficiency and mesh wear*. Powder Technology, 297, 126–143.

JIANG, H., ZHAO, Y., DUAN, C., LIU, C., WU, J., DIAO, H., LV, P., QIAO, J., 2017a. *Dynamic characteristics of an equal-thickness screen with a variable amplitude and screening analysis*. Powder Technology, 311, 239–246.

JIANG, H., ZHAO, Y., QIAO, J., DUAN, C., CHEN, Z., ZHOU, E., DIAO, H., ZHENG, D., 2017b. *Process analysis and operational parameter optimization of a variable amplitude screen for coal classification*. Fuel, 194, 329–338.

HERTZ, H., 1882. *Ueber die Berührung fester elastischer Körper*. 1882, 156–171.

KOPACZ, M., KRYZIA, D., KRYZIA, K., 2017. *Assessment of sustainable development of hard coal mining industry in Poland with use of bootstrap sampling and copula-based Monte Carlo simulation*. Journal of Cleaner Production, 159, 359–373.

LI, H., LIU, C., SHEN, L., ZHAO, L., LI, S., 2021. *Kinematics characteristics of the flip-flow screen with a crankshaft-link structure and screening analysis for moist coal*. Powder Technology, 394, 326–335.

LIAO C., 2016. *Multisized immersed granular materials and bumpy base on the Brazil nut effect in a three-dimensional vertically vibrating granular bed*. Powder Technology, 151-156.

MENBARI A., HASHEMNIA K., 2019. *Effect of vibration characteristics on the performance of mixing in a vertically vibrated bed of a binary mixture of spherical particles*. Chemical Engineering Science, 207: 942 -957.

MORAES, M.N., NOGUEIRA, G.G.R., GALERY, R., MAZZINGHY, D.B., 2022. *Testing a new laboratory-scale high-frequency screen for continuous trials with smaller samples*. Powder Technology, 401, 117286.

VORSTER, W., HINDE, A., SCHIEFER, F., 2002. *Increased screening efficiency using a Kroosher unit coupled with a Sweco screen (Part 1)*. Minerals Engineering, 15, 107–110.

WANG, W., LU, J., WANG, C., YUAN, J., HOU, X., PAN, M., JIANG, H., QIAO, J., DUAN, C., DOMBON, E., ZHAO, Y., 2022. *Study on screening probability model and particle-size effect of flip-flow screen*. Advanced Powder Technology, 33, 103668.

YU, C., LIN, D., XU, N., WANG, X., PU, K., WANG, Z., ZHAO, G., GENG, R., GONG, S., 2023. *DEM simulation of particle flow and separation in a vibrating flip-flow screen*. Particuology, 73, 113–127.

ZHAO L., LI Y., YANG X., et al. 2019. *DEM study of size segregation of wet particles under vertical vibration*. Advanced Powder Technology, 30(7): 1386-1399.25.

ZI, T., ZHANG, H., ZHANG, W., ZHOU, S., BU, X., XIE, G., 2025. *Optimization of external reagent addition on coal slime flotation with compound reagents*. Physicochem Problems of Mineral Processing, 61(2):203300.

WU, B., ZHANG, X., NIU, L., XIONG, X., DONG, Z., TANG, J., 2019. *Research on sieving performance of flip-flow screen using two-way particles-screen panels coupling strategy*. IEEE Access, 7, 124461–124473.

ZHANG, X., WU, B., NIU, L., K., XIONG, X., DONG, Z., 2019. *Dynamic characteristics of two-way coupling between flip-flow screen and particles based on DEM*. Journal of China Coal Society, 1930-1940.

ZHENG, Q.J., XU, M.H., CHU, K.W., PAN, R.H., YU, A.B., 2017. *A coupled FEM/DEM model for pipe conveyor systems: Analysis of the contact forces on belt*. Powder Technology, 314, 480–489.